



ChemComm

---

**Ammonia decomposition mediated at nitrogen vacancies on NaCl-type binary metal nitrides supporting transition metal nanoparticles**

Journal:	<i>ChemComm</i>
Manuscript ID	CC-COM-05-2024-002250.R1
Article Type:	Communication

SCHOLARONE™  
Manuscripts

## Ammonia decomposition mediated at nitrogen vacancies on NaCl-type binary metal nitrides supporting transition metal nanoparticles

Received 00th January 20xx,  
Accepted 00th January 20xx

DOI: 10.1039/x0xx00000x

Masayoshi Miyazaki,<sup>a</sup> Kiya Ogasawara,<sup>a</sup> Yousuke Takekoshi,<sup>a</sup> Kazuki Miyashita,<sup>a</sup> Hitoshi Abe,<sup>b</sup>  
Yasuhiro Niwa,<sup>b</sup> Hideo Hosono<sup>\*, a</sup> and Masaaki Kitano,<sup>\*, a, c</sup>

**Ability of NaCl-type binary transition metal nitrides (incorporating La, Ce, Y, Zr or Hf) to act as catalytic supports facilitating the ammonia decomposition was examined. The effect of nitrogen vacancies formed on nitrides can be understood in terms of the ionic radii of the metal cations. A clear correlation between the N<sub>2</sub> desorption temperature and catalytic activity was found.**

Ammonia is considered a promising hydrogen carrier because it readily undergoes liquefaction under mild conditions and has a higher hydrogen density than other hydrogen carriers such as liquid hydrogen and methylcyclohexane.<sup>1–4</sup> However, building supply chains for on-site ammonia systems will require new ammonia synthesis/decomposition catalysts that work under mild conditions.<sup>5,6</sup> Conventional catalysts typically contain active sites comprising transition metals, and the activities of these materials are limited by scaling relationship, as a consequence of the interactions between nitrogen and the transition metal surfaces.<sup>7–10</sup> Ru has an optimal nitrogen binding energy and is therefore the most active catalyst for both reactions. In addition, ammonia synthesis/decomposition reactions mediated by surface nitrogen vacancies (V<sub>N</sub>) on the support have recently been reported to mitigate scaling limitations.<sup>11–14</sup> The strong interactions between V<sub>N</sub> and nitrogen/ammonia provide adsorption sites on the catalyst support as well as hydrogenation/dehydrogenation sites on the transition metal surfaces. This V<sub>N</sub>-mediated reaction mechanism has enabled the development of non-noble metal catalysts as alternatives to Ru-based catalysts. However,

without clear experimental evidence for V<sub>N</sub> reactivity, we cannot quantitatively discuss the factors determining catalytic performance.

The present study demonstrates the catalysis of ammonia decomposition by NaCl-type binary transition metal nitrides (TMNs, where TM = La, Ce, Y, Zr or Hf). These nitrides are each composed of a metal cation and a nitride anion in a 1:1 molar ratio, resulting in the metal cation existing as an oxide with a charge of 3+. The strength of the interaction between the metal cation and the nitride anion, as provided by the Madelung potential, can be calculated from the ionic radius of the cation,<sup>15–17</sup> and a nitride with a larger lattice constant would be expected to more easily form V<sub>N</sub>. On this basis, the relationship between V<sub>N</sub> formation and catalytic activity can be evaluated using NaCl-type TMNs having various lattice constants. In the present study, the nitrogen desorption onset temperature during N<sub>2</sub>-temperature programmed desorption (TPD) trials is defined as the V<sub>N</sub> formation temperature, and a strong correlation is found between this temperature and the lattice constant of the nitride. Those catalysts with low V<sub>N</sub> formation temperatures exhibited higher ammonia decomposition activity when combined with supported transition metal nanoparticles (M = Ni, Ru, Co or Fe).

Details of the sample preparation procedure and characterization methods are provided in **Supporting Information**. **Figure 1a** shows powder X ray diffraction (XRD) patterns for each nitride and demonstrates that all patterns could be fully indexed to a NaCl-type structure with space group Fm-3m. The lattice constants determined for these nitrides as generated by a Pawley analysis are plotted along with the ionic radii of the 3+ metal cations in **Figure 1b**. The linear correlation between these parameters indicates that LaN and CeN, both of which had large lattice constants, would be expected to have weak interactions between the N<sup>3-</sup> and M<sup>3+</sup> components of the materials. Accordingly, V<sub>N</sub> would be formed more readily on those nitrides having larger lattice constants.

<sup>a</sup> MDX Research Center for Element Strategy, International Research Frontiers Initiative, Tokyo Institute of Technology, 4259 Nagatsuta, Midori-ku, Yokohama 226-8503, Japan. Email: hosono@mces.titech.ac.jp, kitano.m.aa@m.titech.ac.jp

<sup>b</sup> Institute of Materials Structure Science, High Energy Accelerator Research Organization, 1-1, Oho, Tsukuba, Ibaraki 305-0801, Japan.

<sup>c</sup> Advanced Institute for Materials Research (WPI-AIMR), Tohoku University, Sendai 980-8577, Japan.

† Electronic Supplementary Information (ESI) available: Methods for the preparation and characterization of the catalysts and the catalytic properties of the specimens are provided. See DOI: 10.1039/x0xx00000x

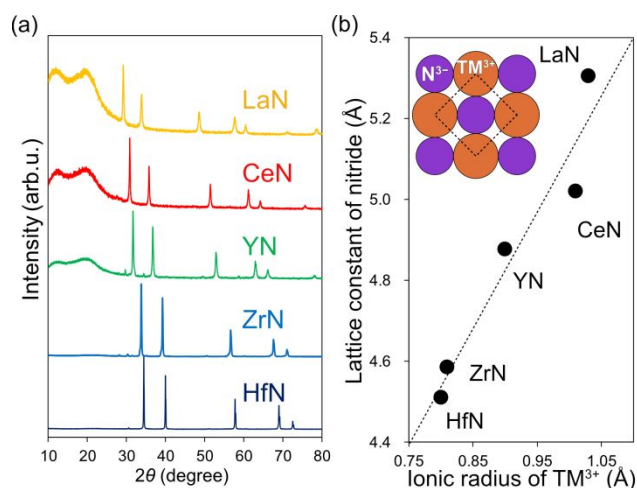


**Figure 1.** (a) XRD patterns for nitrides having NaCl-type structures. (b) Relationship between lattice constant of nitrides and ionic radius of 3+ metal cations.

The presence of  $V_N$  on a number of these nitrides was examined by acquiring  $N_2$ -TPD data, as shown in **Figure 2a**. As previously noted, the onset temperature for  $N_2$  desorption was defined as the  $V_N$  formation temperature in this study (**Figure 2b**). The vacancy formation is generally evaluated by the peak top temperature of TPD profiles, however, the nitrogen detected in such region includes desorbed nitrogen following the diffusion of nitrogen from the bulk to the surface. Therefore,  $V_N$  formation temperature can follow the reactivity of the most active nitrogen at the surface more accurately rather than the amount of nitrogen desorption. As expected from the lattice constants for ZrN and HfN, these materials did not exhibit  $N_2$  desorption below 600 °C, in sharp contrast to LaN and CeN. The  $V_N$  formation temperature was also found to decrease with increasing lattice constant for the TMN (**Figure 2c**). This effect can be explained by the decrease in the Madelung energy associated with an increase in the metal cation radius.<sup>18</sup> Interestingly, CeN showed a much lower  $V_N$  formation temperature than LaN even though the former had a smaller lattice constant. This unique behavior of CeN was attributed to the ready reduction of  $Ce^{3+}$ . The electronic configuration of  $Ce^{3+}$  and  $Ce^{2+}$  in cubic system have been reported to be  $[Xe]4f^1$  and  $[Xe]4f^15d^1$ , respectively.<sup>19,20</sup> According to the band structure of

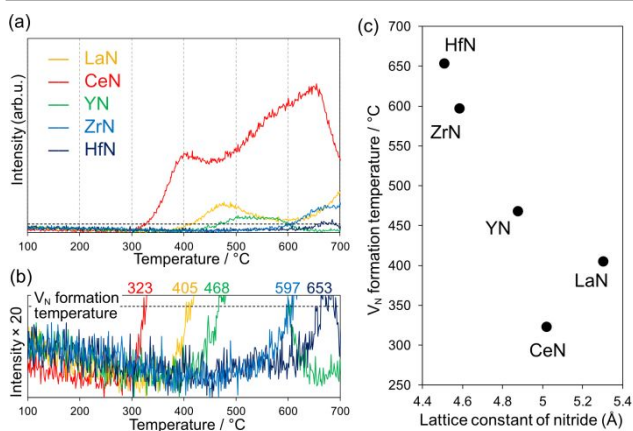


**Figure 2.** (a) TPD profiles for nitrides under He flow based on monitoring at  $m/z = 28$ . (b) Magnified view around baseline in TPD profiles. The  $V_N$  formation temperature was defined as the initial temperature at which  $N_2$  was detected and is indicated. (c)  $V_N$  formation temperature as function of nitride lattice constant.

CeN, unoccupied Ce 5d, which work as the electron acceptor of  $Ce^{3+}$ , cross the Fermi level along  $\Gamma$ -X because of the mixed 4f and 5d character of Ce.<sup>21</sup> On the other hand, the other metal nitrides have indirect band gaps, and the unoccupied d orbital located above Fermi level.<sup>22</sup> As a result,  $Ce^{3+}$  in CeN can accept electrons generated by  $V_N$  formation and promote the formation of  $V_N$  compared to other nitrides. X-ray absorption near-edge structure (XANES) data confirmed that the valence state of Ce was greatly reduced following the introduction of  $V_N$  by exposure to Ar at high temperature, while that of La remained almost unchanged after  $V_N$  formation indicating the electron are trapped at  $V_N$  (**Figure S1**). This suggests that the electron formed by the introducing  $V_N$  delocalized to 5d unoccupied orbital of  $Ce^{3+}$  and reduced to  $Ce^{2+}$ , which hardly not observed in other transition metal nitrides. This effect promoted additional  $V_N$  formation on the CeN, as confirmed by the significant  $N_2$  desorption that was observed (**Figure 2a**). As a result, the  $V_N$  formation temperature for this material deviated from that predicted from the ionic radius of the trivalent cation since the band structure of  $Ce^{3+}$  in CeN crossing the Fermi level mediates the reduction to  $Ce^{2+}$  by the electron. The ammonia decomposition activities and Arrhenius plots of the present Ni-supported nitrides are summarized in **Figure 3a** and **Figure S2**, respectively. The rare-earth nitrides CeN, LaN and YN were found to show enhanced catalytic activity compared with the other specimens. The apparent activation energy ( $E_a$ ) values determined for Ni/CeN, Ni/LaN and Ni/YN were 70, 72 and 81  $\text{kJ}\cdot\text{mol}^{-1}$ , respectively, all of which were lower than those for Ni/ZrN and Ni/HfN (**Figure 3b**). The oxidation states and the coordination numbers for Ni supported on those materials as determined from Ni K-edge X ray adsorption fine structure (XAFS) data were essentially equivalent, and so did not explain

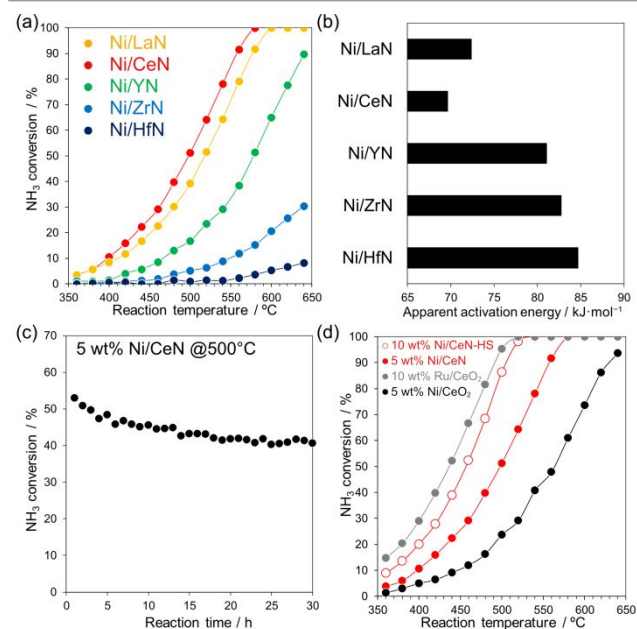


**Figure 3.** (a)  $NH_3$  conversion during ammonia decomposition over 5 wt% Ni/nitrides at WHSV of  $15,000 \text{ mL}_{NH_3}\text{g}_{cat.}^{-1}\text{h}^{-1}$  as function of temperature. (b) Apparent activation energy for ammonia decomposition reaction over various Ni catalysts. (c) Ammonia decomposition over Ni/CeN at 500 °C as function of time. (d) Ammonia decomposition activity over Ni supported on CeN, high-surface-area CeN (CeN-HS), 10 wt% Ru/CeO<sub>2</sub> and 5 wt% Ni/CeO<sub>2</sub> as function of temperature.

the order of activity (Figure S3). Additionally, all nitrides had the similar low specific surface area below  $4 \text{ m}^2 \cdot \text{g}^{-1}$  as summarized in Table S1. These results suggest that the characteristics of the Ni nanoparticles had little effect on catalytic activity, meaning that active sites on the nitride supports determined the catalytic performance. The Ni/CeN exhibited stable activity throughout a 20 h reaction (Figure 3c). An initial gradual degradation of catalytic activity was ascribed to aggregation of the supported Ni particles, verified with XRD patterns after the 24 h reaction (Figure S4). Bare CeN also functioned as a catalyst for ammonia decomposition in the absence of supported Ni, although the catalytic activity increased with increasing Ni loading amount.

This effect plateaued above 5 wt% Ni due to the low surface area of CeN ( $3.5 \text{ m}^2 \cdot \text{g}^{-1}$ ) (Figure S5). It therefore appears that the Ni-CeN interfaces on the material surface served as active sites for ammonia decomposition. To increase the Ni-CeN interface area, a CeN sample having a higher surface area (CeN-HS:  $23.1 \text{ m}^2 \cdot \text{g}^{-1}$ ) was synthesized via nitridation of a  $\text{CeH}_2$  nanopowder made by an arc-evaporation method.<sup>23</sup> A 10 wt% Ni loading on this CeN-HS significantly improved the catalytic activity of the material, providing a performance comparable to that for 10 wt% Ru/CeO<sub>2</sub> (Figure 3d). The hydrogen production rate using Ni/CeN-HS reached  $144.6 \text{ mmol}_{\text{H}_2} \cdot \text{g}_{\text{Ni}}^{-1} \cdot \text{min}^{-1}$  at 500 °C, and this value was similar to values reported for state-of-the-art Ni-based catalysts, as summarized in Table S2. The promotional effect of CeN as a catalyst support was also observed in trials with other transition metals. Figure 4 provides the N<sub>2</sub>-TPD and ammonia decomposition data for M/CeN specimens, where M = Ru, Ni, Co or Fe. The V<sub>N</sub> formation temperature was evidently shifted to lower values by the presence of transition metal nanoparticles on the support, indicating that the formation of V<sub>N</sub> can be initiated at the metal–nitride interfaces. The shift of the V<sub>N</sub> formation temperature by metal loading was also observed in Ni/ZrN (Figure S6). Furthermore, the ammonia decomposition activity for the M/CeN samples was significantly enhanced compared with that for oxide supported catalysts, as can be seen in Figure 4c. The trend exhibited by the catalytic activity and activation energy data (Figure S7) were consistent with that for the V<sub>N</sub>

formation temperature, confirming that V<sub>N</sub> on the nitride support governed catalytic activity. Among the various nitrides, LaN and CeN both showed especially strong ammonia decomposition activity without metal loading (Figure S8). These results indicate that the reactivity of V<sub>N</sub> on the nitrides can dominate the ammonia decomposition performance. The incorporation of V<sub>N</sub> or N<sup>3-</sup> on the nitrides during ammonia decomposition was assessed by performing <sup>15</sup>NH<sub>3</sub> decomposition trials with Ni/CeN (Figure S9). <sup>15</sup>N<sub>2</sub> and <sup>14</sup>N<sup>15</sup>N were observed during the reaction, providing evidence that <sup>14</sup>N<sup>3-</sup> on the CeN was directly involved in the ammonia decomposition reaction. Additionally, the amount of produced <sup>14</sup>N<sup>15</sup>N decreased as the reaction proceeded compared to that of <sup>15</sup>N<sub>2</sub>. This suggests that the <sup>14</sup>N<sup>15</sup>N at the initial reaction period are generated by Ni-Ce<sup>14</sup>N interfacial sites, while those in the later period are due to diffusion from inside the bulk. The lower intensity of <sup>14</sup>N<sup>15</sup>N was attributed to the small surface area of CeN and the large particle size of Ni nanoparticles, yielding the less amount of interface sites than supplied <sup>15</sup>NH<sub>3</sub>. The formation of <sup>14</sup>N<sup>15</sup>N and <sup>15</sup>N<sub>2</sub> in the N<sub>2</sub>-TPD experiments performed after these <sup>15</sup>NH<sub>3</sub> decomposition trials also confirmed the participation of V<sub>N</sub> on the nitrides in the reaction. Moreover, <sup>14</sup>N<sup>15</sup>N production over Ni/CeN was 20 times higher than that obtained for CeN, confirming that ammonia decomposition mediated by V<sub>N</sub> was accelerated at the Ni–CeN support interfaces. The catalytic activity for Ni supported on the various nitrides is plotted against the V<sub>N</sub> formation temperature for the nitrides in Figure 5a. The evident linear correlation demonstrates that potential of V<sub>N</sub> formation on the nitride supports determined the level of catalytic activity. Ce<sup>3+</sup> and La<sup>3+</sup> (both having large ionic radii) appear to have promoted V<sub>N</sub> formation, leading to the superior catalytic performance of Ni/CeN and Ni/LaN. This trend was also evident in data obtained from a series of CeN specimens incorporating different transition metals (Figure 5b). Ru/CeN, which produced V<sub>N</sub> at the lowest temperature, exhibited the highest activity. The enhanced catalytic activity resulting from transition metal loading can be explained by accelerated V<sub>N</sub> formation at the metal–CeN support interfaces. The formation of V<sub>N</sub> on nitrides

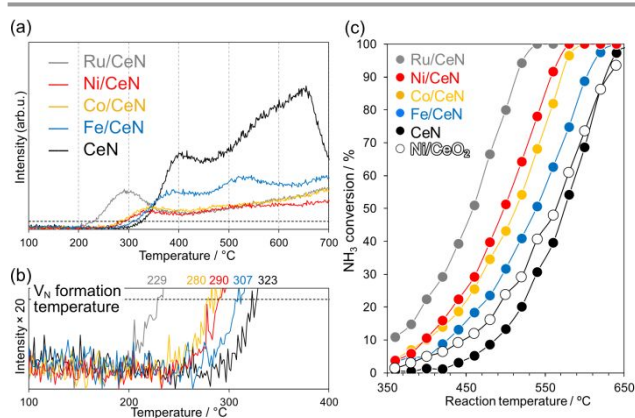


**Figure 4.** (a) TPD profiles for M/CeN under He flow based on monitoring at  $m/z = 28$  (M = Ru, Ni, Co or Fe). (b) Magnified view around baseline in TPD profiles, with V<sub>N</sub> formation temperature indicated. (c) NH<sub>3</sub> conversion during ammonia decomposition over 5 wt% M/CeN at WHSV of  $15,000 \text{ mL}_{\text{NH}_3} \cdot \text{g}_{\text{cat}}^{-1} \cdot \text{h}^{-1}$  as function of temperature.

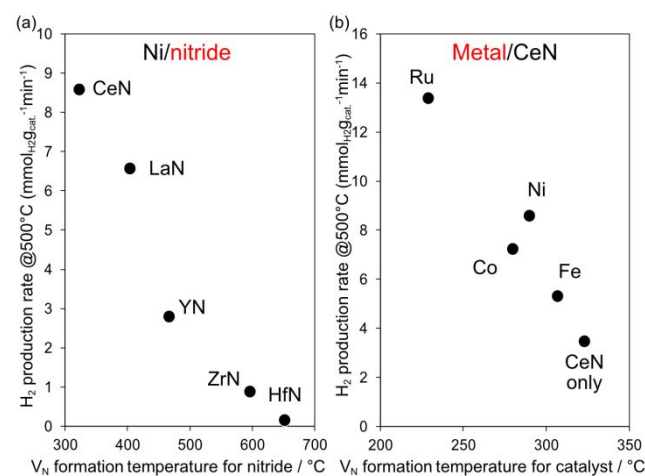


**Figure 5.** H<sub>2</sub> production rate during ammonia decomposition reaction at 500 °C as function of V<sub>N</sub> formation temperature for trials with (a) Ni/nitride and (b) M/CeN.

was also modeled using DFT calculations, employing a slab model structure. The  $V_N$  formation energies calculated for the nitrides closely matched the experimental results and were consistent with the lattice constants as well as the  $V_N$  formation temperatures for the nitrides (Figure 6a). There was additionally a strong correlation between the calculated  $V_N$  formation energy and the catalytic activity of the Ni/nitrides specimens, as shown in Figure 6b, similar to that observed for the experimental  $V_N$  formation temperatures. In addition, the charge of Ce on CeN determined from Bader Charge analysis<sup>24</sup> was reduced with the  $V_N$  formation, consistent with the facilitated reduction of  $Ce^{3+}$  to  $Ce^{2+}$  promoting the  $V_N$  formation (Figure S10).

The present experimental and theoretical results indicate that the catalytic performance of these nitride-supported catalysts during ammonia decomposition was determined by the reactivity of  $V_N$  at the metal–nitride interfaces. As demonstrated in our previous work, increased catalytic activity due to  $V_N$  on the support can be explained by the desorption of lattice  $N^{3-}$  as  $N_2$  gas via supported metal nanoparticles and by ammonia adsorption on cation sites adjacent to  $V_N$  sites.<sup>13,14</sup> The associated ammonia decomposition mechanism can be summarized as follows. Initially, lattice  $N^{3-}$  on the nitride support is desorbed as  $N_2$  gas to form  $V_N$  sites (step I). Ammonia molecules are immediately adsorbed on the electropositive cation sites adjacent to  $V_N$  sites (step II). The N–H bonds of these adsorbed  $NH_3$  molecules are activated by surrounding supported metals to form  $NH_x$  species in conjunction with  $H_2$  gas generation (step III). Following the complete dehydrogenation of ammonia, N adatoms on the cation sites refill the  $V_N$  sites to form lattice  $N^{3-}$ . In conclusion, transition metal nanoparticles promoted the formation of  $V_N$  on the nitride support, resulting in the high catalytic activity observed during the ammonia decomposition reaction.

This work was supported by the FOREST Program (grant no. JPMJFR203A) of the Japan Science and Technology Agency (JST) and by KAKENHI grants-in-aid (nos. JP20K22550, JP22H00272, JP22K18914 and JP23K13600) from the Japan Society for the Promotion of Science (JSPS). A part of this work was also supported by the JST-Mirai Program (grant no. JPMJMI21E9) funded by JST and by the Tokuyama Science Foundation. The

XASf analyses were conducted with the approval of PF-PAC (project no. 2019G503).

## Conflicts of interest

There are no conflicts to declare.

## Notes and references

- N. Salmon and R. Bañares-Alcántara, *Sustainable Energy Fuels*, 2021, **5**, 2814–2839.
- C. Zamfirescu and I. Dincer, *Fuel Processing Technology*, 2009, **90**, 729–737.
- R. M. Nayak-Luke and R. Bañares-Alcántara, *Energy Environ. Sci.*, 2020, **13**, 2957–2966.
- D. R. MacFarlane, P. V. Cherepanov, J. Choi, B. H. R. Suryanto, R. Y. Hodgetts, J. M. Bakker, F. M. Ferrero Vallana and A. N. Simonov, *Joule*, 2020, **4**, 1186–1205.
- J. Armijo and C. Philibert, *International Journal of Hydrogen Energy*, 2020, **45**, 1541–1558.
- S. F. Yin, B. Q. Xu, X. P. Zhou and C. T. Au, *Applied Catalysis A: General*, 2004, **277**, 1–9.
- C. J. H. Jacobsen, S. Dahl, B. S. Clausen, S. Bahn, A. Logadottir and J. K. Nørskov, *Journal of the American Chemical Society*, 2001, **123**, 8404–8405.
- A. J. Medford, J. Wellendorff, A. Vojvodic, F. Studt, F. Abild-Pedersen, K. W. Jacobsen, T. Bligaard and J. K. Nørskov, *Science*, 2014, **345**, 197–200.
- A. Boisen, S. Dahl, J. Nørskov and C. Christensen, *Journal of Catalysis*, 2005, **230**, 309–312.
- D. A. Hansgen, D. G. Vlachos and J. G. Chen, *Nature Chemistry*, 2010, **2**, 484–489.
- H. Jin, L. Li, X. Liu, C. Tang, W. Xu, S. Chen, L. Song, Y. Zheng and S. Qiao, *Advanced Materials*, 2019, **31**, 1902709.
- T.-N. Ye, S.-W. Park, Y. Lu, J. Li, M. Sasase, M. Kitano, T. Tada and H. Hosono, *Nature*, 2020, **583**, 391–395.
- K. Ogasawara, T. Nakao, K. Kishida, T. N. Ye, Y. Lu, H. Abe, Y. Niwa, M. Sasase, M. Kitano and H. Hosono, *ACS Catalysis*, 2021, **11**, 11005–11015.
- K. Ogasawara, M. Miyazaki, K. Miyashita, H. Abe, Y. Niwa, M. Sasase, M. Kitano and H. Hosono, *Advanced Energy Materials*, 2023, **13**, 2301286.
- M. O’Keeffe, *Acta Crystallogr A Cryst Phys Diffr Theor Gen Crystallogr*, 1979, **35**, 776–779.
- E. C. Baughan, *Trans. Faraday Soc.*, 1959, **55**, 2025–2029.
- D. H. Gregory, *J. Chem. Soc., Dalton Trans.*, 1999, 259–270.
- R. Ouyang, *Chem. Mater.*, 2020, **32**, 595–604.
- R. Visser, J. Andriessen, P. Dorenbos and C. W. E. Eijk, *J. Phys.: Condens. Matter*, 1993, **5**, 5887–5910.
- N. Popov, A. Mysovsky, R. Shendrik and E. Radzhabov, *Radiation Measurements*, 2016, **90**, 55–58.
- P. Larson, W. R. L. Lambrecht, A. Chantis and M. Van Schilfgaarde, *Phys. Rev. B*, 2007, **75**, 045114.
- A. J. E. Rowberg, S. Mu, M. W. Swift and C. G. Van De Walle, *Phys. Rev. Materials*, 2021, **5**, 094602.
- Y. Lu, J. Li, T. N. Ye, Y. Kobayashi, M. Sasase, M. Kitano and H. Hosono, *ACS Catalysis*, 2018, **8**, 11054–11058.
- W. Tang, E. Sanville and G. Henkelman, *Journal of Physics: Condensed Matter*, 2009, **21**, 084204.

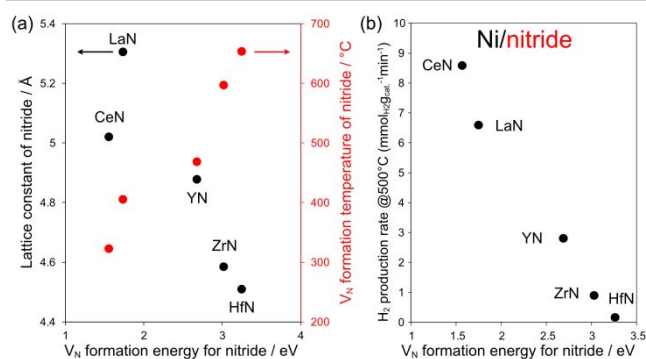


**Figure 6.** Lattice constant and  $V_N$  formation temperature for various nitrides as function of calculated  $V_N$  formation energies for nitrides. (b)  $H_2$  production rates during ammonia decomposition reaction at 500 °C as function of  $V_N$  formation temperature for Ni/nitrides.